Highly photosensitive thin film transistors based on a composite of poly(3-hexylthiophene) and titania nanoparticles

Feng Yan,[a] Jinhua Li, and Sheung Man Mok
Department of Applied Physics, The Hong Kong Polytechnic University, Kowloon, Hong Kong SAR, China

(Received 26 May 2009; accepted 17 August 2009; published online 2 October 2009)

Organic phototransistors based on a composite of P3HT and TiO_2 nanoparticles have been fabricated, which show high photosensitivity, fast response, and stable performance under both visible and ultraviolet light illumination, and thus they are promising for applications as low cost photosensors. The transfer characteristic of each device exhibits a parallel shift to a positive gate voltage under light illumination, and the channel current increases up to three orders of magnitude in the subthreshold region. The shift in the threshold voltage of the device has a nonlinear relationship with light intensity, which can be attributed to the accumulation of electrons in the embedded TiO_2 nanoparticles. It has been found that the device is extremely sensitive to weak light due to an integration effect. The relationship between the threshold voltage change and the intensity of light illumination can be fitted with a power law. An analytical model has been developed to describe the photosensitive behavior of the devices. It is expected that such organic phototransistors can be developed for sensing different wavelengths based on different semiconducting polymers and semiconducting nanoparticles. © *2009 American Institute of Physics*. [doi:10.1063/1.3225760]

I. INTRODUCTION

Organic semiconductor materials, including small molecules and polymers, have gained considerable interest recently for their broad potential applications in the electronics and semiconductor industry. Organic thin film transistors (OTFTs) have a broad range of applications, including flexible displays, sensors, wearable electronics, smart packages, memories, radio frequency identification tags,[1] etc. It has been recognized that thin film transistors offer a great deal of promise for applications in various types of sensors, including light sensor,[2,3] pressure sensor,[4] gas sensor,[5] and chemical, biological, and medical sensors.[6–9] Miniaturization is demanded for all types of sensors because of the need for better portability, higher sensitivity, lower power dissipation, and better device integration. OTFTs can be miniaturized without a reduction in signal to noise ratio since the channel current is not directly related to the area but to the ratio between the channel width and length of the device.[10] Moreover, OTFTs can be fabricated using low-temperature solution processes on a variety of substrates, including mechanically flexible ones. Since various printing techniques have been well developed,[11] miniaturization of these devices is straightforward, and thus portability, small sample volume, and arrays with many elements are achievable. Also, a sensor based on a transistor can be integrated in a circuit and provide a response that can be easily measured.

Phototransistors are a type of optical transducer in which light detection and signal amplification are combined in a single device.[12] Organic phototransistors (OPTs) are considered to be one of the feasible applications of OTFTs because of the strong light absorption and the excellent photocurrent generation efficiency of organic semiconductors. More importantly, OPTs can be easily integrated into flexible electronic products and biological systems as light sensors or biosensors.

There are two types of OPTs that have been developed based on semiconducting oligomers and polymers. One type is based on the mechanism of trapping excited electrons at the insulator/semiconductor interface of the device under light illumination, which normally induces a positive shift of the threshold voltage of the device. OPTs fabricated by thermal evaporation of some oligomers including pentacene,[13–16] rubrene,[17] and others[18–20] are this type of devices. In addition, solution processible OPTs based on conjugated polymers, such as poly(9,9-dioctylfluorene-co-bithiophene) (F8T2) (Ref. 21) and poly(3-octylthiophene-2,5-diyl) (P3OT),[22] have been reported with the same working mechanism. However, trap states at the insulator/semiconductor interface may induce an obvious bias stressing effect.[13] Therefore, the photosensitive behavior of this type of phototransistor is normally associated with an unstable performance, which will be a shortcoming in its real application.

Another type of OPT is based on a composite film of *n*-type and *p*-type semiconductors, such as the composite of poly[2-methoxy-5-(3,7-dimethyloctyloxy)]-1,4-phenylenevinylene) and methanof (6,6)-phenyl C_{61}-butyric acid methyl ester,[23] which is normally used in a photovoltaic device. The photosensitive behavior of such device is due to the charge generated by absorbed photons. However, a poor performance has been observed in this type of device due to a much higher off current induced by a photovoltaic effect.

Composite films of poly(3-hexylthiophene) (P3HT) and TiO_2 nanoparticles have been used in solar cells, which show relatively low power conversion efficiency due to poorly formed conduction paths for electrons.[24,25] But we find that such composite films have special advantages for the applications in OPTs since the TiO_2 nanoparticles can store

[a]Electronic mail: apafyan@polyu.edu.hk.

charge (electrons) under light illumination. Recently, we have reported a new type of OPT based on a composite film of P3HT and TiO_2 nanoparticles.[3] The device shows a quick change in channel current under light illumination, which can be attributed to a positive shift in the threshold voltage, while no change in the field effect mobility and off current can be observed. In addition, the device shows very stable performance under a light illumination, which is very important for its application. However, the maximum change in the threshold voltage of the OPTs that we have reported before is only several volts. Therefore, the fabrication process of the OPTs needs to be optimized to increase the sensitivity.

In this paper, we will report that the sensitivity of the device can be improved for one order of magnitude by carefully choosing the TiO_2 nanoparticles. The device shows high photosensitivity under the illumination of both visible and ultraviolet (UV) light, and thus it is promising in the applications as photosensors, especially for UV sensors. Also, the sensing mechanism of the OPTs has been carefully studied in this paper. An analytical model for the photosensitive behavior of the OPTs is developed in this paper.

II. EXPERIMENTAL

Regioregular P3HT with head-to-tail linkages of 90%–93% was purchased from Rieke Metals Inc. and was used as received without additional purification. TiO_2 nanopowder with different grain sizes and phases (anatase or rutile) were purchased from Sigma-Aldrich. P3HT and TiO_2 powders are dissolved in toluene and stirred for 24 h before being spin-coated on a substrate.

High-resolution transmission electron microscopy (HRTEM) (JEOL JEM-2010) was used to characterize the morphology of the TiO_2 nanoparticles and the P3HT and TiO_2 composite films. To prepare samples for TEM study, P3HT and TiO_2 composite films were spin-coated on glass substrates under the same fabrication condition of OPTs and then peeled with a bistoury and collected by copper grids. TiO_2 nanoparticles with different grain sizes and phases were dispersed in ethanol and collected with copper grids for TEM observation. Figure 1 shows the TEM images of the TiO_2 nanoparticles and the P3HT and TiO_2 composite films. The distributions of TiO_2 nanoparticles in the P3HT matrix are shown in (g), (h), and (i). Some clusters of nanoparticles can be observed in the three composite films. The phases of the TiO_2 nanoparticles were confirmed by electron diffraction patterns and lattice spaces in HRTEM images.

An OPT is fabricated on a SiO_2/n -type Si substrate, as shown in the inset of Fig. 2(a). The resistivity of the n-type Si is 0.001 Ω cm. The thickness of the SiO_2 is 500 nm. Au source/drain electrodes are deposited through a shadow mask on top of the SiO_2 film by thermal evaporation. Then, a bottom-gate-bottom-contact OTFT is fabricated by spin-coating a layer of composite film of P3HT and TiO_2 nanoparticles. The device is annealed at 100 °C for 2 h in a glovebox filled with high purity N_2. The channel width and length of the device are 2000 and 200 μm, respectively. Devices with different weight ratios between P3HT and TiO_2 have been fabricated to find the most photosensitive composition, as shown in Table I.

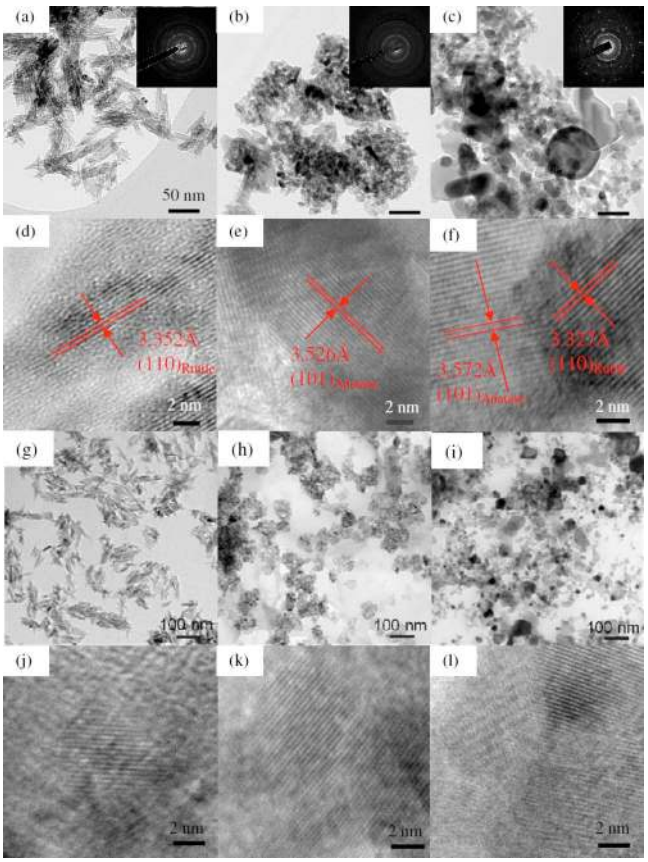

FIG. 1. (Color online) [(a), (b), and (c)] TEM images of TiO_2 nanoparticles with rutile, anatase, and mixture of rutile and anatase phases, respectively. [(d), (e), and (f)] HRTEM images of different TiO_2 nanoparticles shown in (a), (b), and (c), respectively. [(g), (h), and (i)] TEM images of composite films of P3HT and TiO_2 nanoparticles with rutile, anatase, and mixture of rutile and anatase phases, respectively. Weight ratio of P3HT:TiO_2 =1:0.75. [(j), (k), and (l)] Magnified views of (g), (h), and (i), respectively.

All of the devices are measured in a glovebox with a semiconductor parameter analyzer (Agilent 4156 C). Light emission diodes [wavelength $\lambda = \sim 370$ nm (UV) and 470, 530, and 590 nm] driven by a wave form generator (Agilent 33220 A) are used as light sources.

III. RESULTS AND DISCUSSION

Figure 2(a) shows the transfer curves ($I_{DS} \sim V_{GS}$) of an OPT (sample 1, the average dimension of TiO_2 grains with a rutile phase is 5×20 nm^2, with a weight ratio of P3HT:TiO_2=1:0.75) measured under illumination of UV light (the wavelength λ is ~370 nm). The transfer curve shows a parallel shift to positive values under the light illumination, and the voltage shift increases with an increase in light intensity. The device shows a similar photosensitive behavior to different wavelengths. Figure 2(b) shows the transfer characteristics of the sample under light illumination with a wavelength of 530 nm. It is worth noting that the channel current changes for more than three orders of magnitude in the subthreshold region. The small change in the off current and the subthreshold slope of the device under light

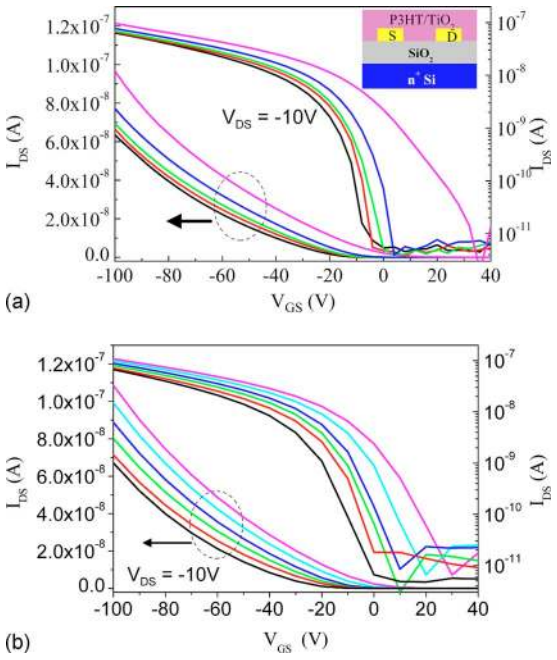

FIG. 2. (Color online) Transfer characteristics of an OPT based on a composite of P3HT and TiO_2 nanoparticles measured under light illumination [sample 1, weight ratio of P3HT:TiO_2=1:0.75, grain size of TiO_2 (rutile): 5×20 nm^2]. (a) The wavelength of the light is ~370 nm (UV). From left to right, the curves are measured at the light intensities of 0, 1.55, 18.06, 48.98, and 1580 $\mu W/cm^2$. Inset: cross sectional view of the OPT. (b) The wavelength of the light is 530 nm. From left to right, the curves are measured at the light intensities of 0, 0.14, 2.6, 6.7, 12.8, and 38.4 $\mu W/cm^2$.

illumination can be attributed to the photocurrent generated in the composite film. The on/off ratio of the device is kept at $\sim10^4$ under light illumination since the photocurrent is relatively low.

We have found that the grain size and the weight fraction of TiO_2 nanoparticles are of paramount importance for the photosensitivity. Table I shows the shifts in the threshold voltages of the OPTs with different grain sizes and weight fractions of TiO_2 nanoparticles measured under light illumination with the same light intensity and wavelength (intensity: 10 $\mu W/cm^2$; wavelength: 530 nm). It can be found that sample 1 shows the maximum photosensitivity, which can be attributed to the needlelike shape of the TiO_2 nanoparticles

TABLE I. Shift in the threshold voltages (ΔV_{th}) of OPTs based on P3HT/TiO_2 composite films measured under the light illumination of 10 $\mu W/cm^2$ (wavelength: 530 nm). β and A are parameters for the best fitting of Eq. (1) in Fig. 4(b).

Sample number	TiO_2 grain size	Weight fraction of P3HT:TiO_2	ΔV_{th} (V)	β	A
1	5×20 nm^2 (rutile)	1:0.75	18.69	0.347	7.898
2		1:0.5	6.36	0.275	3.320
3		1:0.25	2.68	0.241	1.527
4	10 nm (anatase)	1:0.75	2.78	0.298	1.382
5	10–100 nm	1:0.75	1.52	0.347	0.653
6	(mixture of rutile	1:1	1.67	···	···
7	and anatase)	1:0. 5	1.27	···	···
8		1:0.25	0.56	···	···

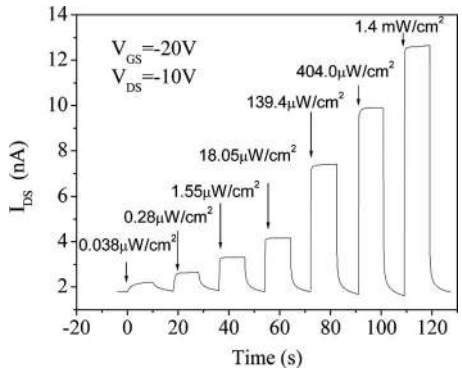

FIG. 3. The channel current of an OPT (sample 1) based on a composite of P3HT and TiO_2 nanoparticles measured under light illumination (UV, λ =370 nm) with different intensities. Weight ratio of P3HT:TiO_2=1:0.75; average grain size of TiO_2 (rutile): 5×20 nm^2.

that can increase the interface area between P3HT and TiO_2. With the increase in the weight fraction of TiO_2 nanoparticles, the photosensitivity of the device increases while the channel current decreases since TiO_2 nanoparticles prohibit hole transfer in the channel. On the other hand, we observed that the films with a higher weight fraction of TiO_2 are not uniform and big clusters of TiO_2 nanoparticles are formed in the composite film. Therefore, we normally choose a weight ratio of P3HT:TiO_2=1:0.75 as an optimum ratio for the device.

The response time of an OPT to light illumination is an important parameter for its applications. OPTs that have been reported before normally show a response time of more than 10 s since the trapping process of electrons at the semiconductor/insulator interface is relatively slow.[13,20,22] It is worth noting that the OPTs reported in this paper show a much faster response to light illumination due to a different sensing mechanism, which will be explained later. As shown in Fig. 3, the channel current of an OPT (sample 1) was measured at fixed gate and drain voltages (V_{GS}=−20 V, V_{DS}=−10 V) under illumination of UV light. Since the light emission diode can be switched on and off in tens of nanoseconds, the change in the channel current will present the response behavior of the OPT to light illumination. The channel current increases sharply to a stable value when the light is switched on and changes back to its original value when the light is switched off. Therefore, the device performance is very stable and reliable under light illumination.

Figure 4(a) shows the shift in the threshold voltage of sample 1 under light illumination, which is decided by measuring transfer characteristics. It can be found that the photosensitivity is approximately proportional to the light absorbance of the composite film at different wavelengths, as shown in the inset of Fig. 4(a). The device is extremely sensitive to weak light, and the shift in the threshold voltage (ΔV_{th}) shows a nonlinear relationship with light intensity (I), which can be fitted very well with a power law,

$$\Delta V_{th} = AI^{\beta}, \tag{1}$$

where β is the power factor, which varies between 0.2 and 0.4 for different wavelengths of the incident light. Table II shows the fitting parameters A and β for sample 1 illumi-

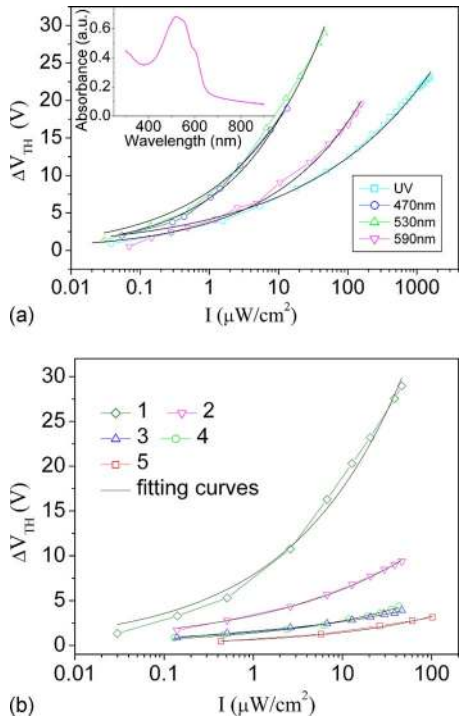

FIG. 4. (Color online) (a) Shift in the threshold voltage ΔV_{th} of sample 1 under light illumination with different wavelengths. (b) Shift in the threshold voltage ΔV_{th} of samples 1–5 under light illumination with a wavelength of 530 nm. Black solid curves in (a) and (b) show the best fitting with the equation $\Delta V_{th}=AI^{\beta}$.

nated with different wavelengths. Figure 4(b) shows the photosensitivity of different devices (samples 1–5) to the light with a wavelength of 530 nm, and the curves are fitted with Eq. (1). The fitting parameters A and β are shown in Table I.

Next, we will explain the sensing mechanism of the OPTs. The energy diagram of the P3HT/TiO_2 composite ($E_{LUMO}<E_C<E_{HOMO}<E_V$) is shown in Fig. 5, where E_{LUMO} and E_{HOMO} are the energy levels of the lowest unoccupied molecular orbital (LUMO) and the highest occupied molecular orbital (HOMO) of P3HT, respectively; E_V and E_C are the energy levels of the valence band and the conduction band of TiO_2, respectively. So, a type-II heterojunction structure (staggered gap) is formed in the P3HT/TiO_2 composite. More importantly, an exciton generated by a photon absorbed by P3HT or TiO_2 will dissociate into an electron and a hole when the exciton moves to the P3HT/TiO_2 interface since the energy decrease of the electron or hole is larger than the binding energy of the exciton (electron-hole pair). Under visible light, excitons are generated in the P3HT part. Electrons generated by the dissociation of the excitons at the interface will be trapped in the TiO_2 nanoparticles. While under UV illumination, excitons are generated in the TiO_2 nanoparticles. After the dissociation of the excitons, the

TABLE II. Parameters for the best fitting of the shift in the threshold voltage vs light intensity (different wavelengths) with Eq. (1) in Fig. 4(a).

Wavelength	UV	470 nm	530 nm	590 nm
A	4.154	6.962	7.898	4.012
β	0.237	0.397	0.347	0.314

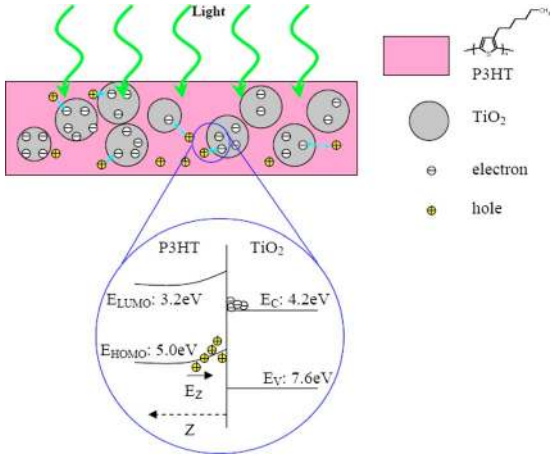

FIG. 5. (Color online) Schematic diagram showing charge accumulation in a P3HT/TiO_2 composite film under light illumination.

holes diffuse to the P3HT part and the electrons remain in the nanoparticles. Therefore, light illumination can result in electrons accumulated in TiO_2 nanoparticles in both cases, which will change the threshold voltage of the OPTs.

The density of accumulated electrons in TiO_2 nanoparticles is controlled by the following process. Under light illumination, electrons are generated in the TiO_2 nanoparticles due to the dissociation of excitons at the P3HT/TiO_2 interface. On the other hand, electrons will recombine with holes at the interface. Therefore, a balance will be reached after a certain density of electrons accumulated in the TiO_2 nanoparticles. The time taken to arrive at a stable state is the response time of the OPT. During the accumulation of electrons in the TiO_2 nanoparticles, a potential barrier and a buildup electric field will be formed at the P3HT/TiO_2 interface, which will increase the recombination rate of electrons and holes at the interface, as shown in Fig. 5.

Since the transfer characteristics of an OPT shows a parallel shift under light illumination, the transient behavior of the threshold voltage of an OPT can be calculated according to the change in the channel current of the device measured at a fixed working voltage under light illumination. Figure 6(a) shows the change in the threshold voltage of sample 1 measured when the light illumination is switched on and off. The rising edge can be fitted very well with an exponential function: $\Delta V_{th}(t)=\Delta V[1-\exp(-t/\tau)]$ for low light intensity, where τ is the response time of the device. When the response time is shorter than ~10 ms, it is too fast to be measured by the semiconductor parameter analyzer. Figure 6(b) shows the response time τ of sample 1, which decreases rapidly with an increase in light intensity. The response time can be regarded as the integration time of the sensing process, and therefore the device shows higher sensitivity to lower light intensity due to an integration effect.

The recovery of the threshold voltage after the light is switched off can be fitted with an exponential function with at least two relaxation times: $\Delta V_{th}(t)=\Delta V_1 \exp[(t_0-t)/\tau_1]+\Delta V_2 \exp[(t_0-t)/\tau_2]$, where ΔV_1 and ΔV_2 are constants and τ_1 and τ_2 are relaxation times, as shown in Fig. 6(a). Normally, the current drops to a lower value in several milliseconds and then slowly decays to a stable value in several

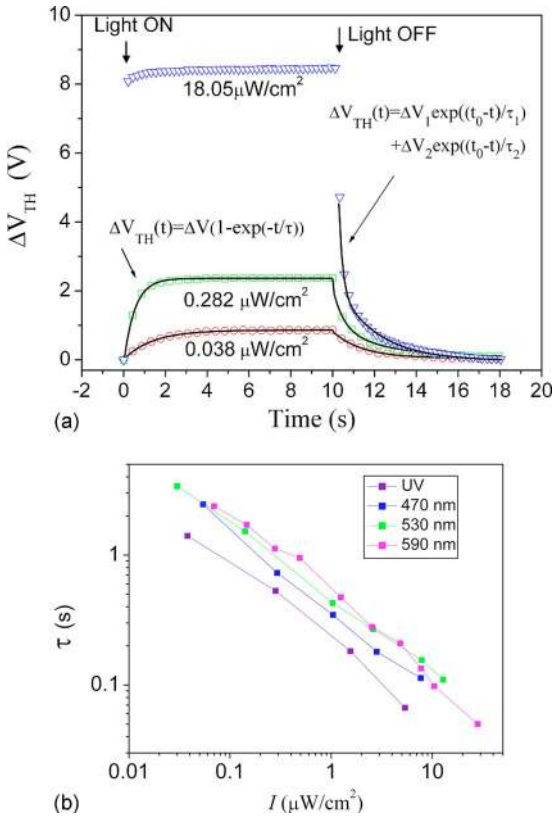

FIG. 6. (Color online) (a) The change in the threshold voltage (ΔV_{th}) of an OPT (sample 1) measured under UV light illumination with different intensities. From top to bottom, the light intensities are 18.05, 0.282, and 0.038 $\mu\text{W/cm}^2$, respectively. Black solid curves show the best fitting with $\Delta V_{\text{th}}(t)=\Delta V[1-\exp(-t/\tau)]$ for rising edges and $\Delta V_{\text{th}}(t)=\Delta V_1 \exp[(t_0-t)/\tau_1]+\Delta V_2 \exp[(t_0-t)/\tau_2]$ for falling edges. (b) Response time τ for different light intensities and wavelengths.

seconds. The first stage can be regarded as the recombination of electrons and mobile holes at the P3HT/TiO_2 interface, while the second is probably due to the recombination of electrons and trapped holes near the interface. Since the trap states have different capture cross sections and energy levels, the recovery process will show a broad distribution of relaxation time.[26]

We consider that electrons accumulated in the TiO_2 nanoparticles will decrease the electrostatic potential of the active layer (P3HT/TiO_2 composite film) and thus change the threshold voltage of the device, as shown in Fig. 7. The threshold voltage V_{th} of a p-type OTFT is given by

$$V_{\text{th}} = V_{\text{fb}} - \psi_B - \frac{\sqrt{2\varepsilon_s q N_D \psi_B}}{C_i}, \tag{2}$$

where ψ_B is the electrostatic potential in the active layer (ψ_B is also the potential difference between the HOMO and the Fermi level of the semiconducting polymer), N_D is the effective doping level of the organic semiconductor, ε_s is the dielectric constant of the semiconductor, C_i is the capacitance of the gate insulator per unit area, and V_{fb} is the flatband voltage of the device. Therefore, the threshold voltage V_{th} will increase with a decrease in ψ_B.

It is worth noting that the device sensitivity is related to the ability of trapping charge in TiO_2 nanoparticles. Obviously, the interface area and dispersion level of TiO_2 nanoparticles in the P3HT matrix are very important factors for the device sensitivity. In addition, there are many other important factors needed to be considered. One is the density of trap states in the TiO_2 nanoparticles, which is dependent on the fabrication process and is difficult to be directly characterized. Another important factor can be the different physical properties of TiO_2 with different phases. Although TiO_2 with the anatase phase shows better effect in solar cells than the rutile phase, which is normally attributed to higher electron mobility in the anatase phase,[27] we cannot find a relationship between the ability of trapping charge and electron mobility in the TiO_2 nanoparticles. Therefore, it is difficult to attribute the different photosensitivities of the devices to distinct physical properties of different phases at this stage, and further work is needed to better understand it.

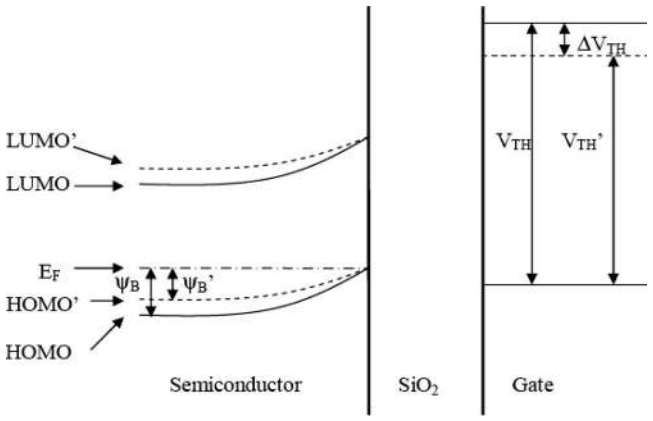

FIG. 7. Energy-band diagrams for an OPT under gate biases of its threshold voltage. The threshold voltages of the device, V_{th} and V'_{th}, correspond to different electrostatic potentials of the active layer, ψ_B and ψ'_B, respectively.

An analytical model for the OPTs under a weak light illumination can be developed as follows. We may assume that the change in electrostatic potential $\Delta\psi_B$ is approximately proportional to the density of electrons accumulated in the TiO_2 nanoparticles (Q_e). Taking a first order approximation, we will get the change in the threshold voltage given by

$$\Delta V_{\text{th}} \propto \Delta\psi_B \propto Q_e. \tag{3}$$

A potential barrier will be formed at the P3HT/TiO_2 interface under light illumination due to the accumulated electrons and holes near the P3HT/TiO_2 interface. Since the field effect mobility of holes in P3HT is much lower than that of electrons in TiO_2 and the density of trap states in P3HT is much higher than that in TiO_2, we will only consider the effect of the buildup electric field in the P3HT part. The distribution of the electric field component normal to the interface E_z is found from the solution of Poisson's equation,

$$\frac{dE_z}{dz} = \frac{\rho}{\varepsilon_s}, \tag{4}$$

where z is the space coordinate (perpendicular to the interface) and ρ is the space charge density,

$$\rho = qp, \tag{5}$$

where q is the electronic charge and p is the concentration of holes in the HOMO level of P3HT. We will assume that the density of trap states above the HOMO level of P3HT is given by[28,29]

$$N(E) = N_G \exp[(E - E_V)/kT_d], \tag{6}$$

where N_G, E_V, and T_d (the characteristic temperature) are constants and k is the Boltzmann constant. Therefore, the hole density is given by

$$p(V) = qp_0 \exp(-V/kT_d), \tag{7}$$

where p_0 is the hole density in P3HT with zero internal electric field and V is the potential change in P3HT induced by an internal electric field ($V<0$).

Using the relationship between the electric field perpendicular to the P3HT/TiO_2 interface and the potential near the interface,

$$E_z = \frac{dV}{dz}. \tag{8}$$

We will find from Poisson's equation,

$$\begin{aligned} |E_{z=0}| &= \left[\left(\frac{2}{\varepsilon_s} \right) \left| \int_{\psi}^{0} \rho(V')dV' \right| \right]^{1/2} \\ &= \left\{ \frac{2qp_0kT_d}{\varepsilon_s} [\exp(-\psi/kT_d) - 1] \right\}^{1/2} \\ &\approx \sqrt{\frac{2qp_0kT_d}{\varepsilon_s}} \exp(-\psi/2kT_d), \end{aligned} \tag{9}$$

where V' varies from zero (far away from the interface) to potential ψ ($\psi<0$) at the P3HT/TiO_2 interface and $E_{z=0}$ is the electric field in P3HT near the interface. Therefore, the charge (electrons) density accumulated in TiO_2 per unit interface area (n_t) is given by

$$n_t = \frac{\varepsilon_s}{q}|E_{z=0}| = \sqrt{\frac{2p_0\varepsilon_skT_d}{q}} \exp(-\psi/2kT_d) \propto Q_e. \tag{10}$$

The recombination rate (γ) of electrons with holes at the P3HT/TiO_2 interface is

$$\gamma = \eta_{re} n_t p(\psi) = \eta_{re} p_0 \sqrt{\frac{2p_0\varepsilon_skT_d}{q}} \exp\left(\frac{-3\psi}{2kT_d} \right) \propto Q_e^3, \tag{11}$$

where η_{re} is the recombination coefficient of electrons and holes at the interface.

The generation rate of electrons at the interface should be equal to the recombination rate of electrons when a balance is arrived; therefore,

$$\gamma = I \frac{\Gamma(\lambda)\lambda}{hc} \eta \propto I, \tag{12}$$

where I is the light intensity, $\Gamma(\lambda)$ is the light absorbance of the semiconductor layer (P3HT for visible light and TiO_2 for UV light) at the wavelength of λ, η is the overall quantum efficiency of charge generation at the interface, c is the speed of light in vacuum, and h is the Planck constant. Here, we assume that the charge separation coefficient of excitons at the P3HT/TiO_2 interface is not dependent on the electric field at the interface.[30] Then, we will obtain

$$\Delta V_{th} \propto I^{1/3}, \tag{13}$$

which is Eq. (1) with a power factor of 1/3. Although the above analytical model is based on a first order approximation, the experimental results fitted with Eq. (1) show power factors very close to 1/3, as shown in Tables I and II.

Based on the above principle, OPTs based on composites of various semiconducting polymers and semiconducting nanoparticles can be developed as photosensors for different purposes. To realize a device sensitive to a broader range of wavelengths, we can choose different inorganic nanoparticles that are sensitive to different wavelengths from the infrared to the UV region, which are readily available in the market.

IV. CONCLUSIONS

In conclusion, we have developed a new type of light sensitive OTFTs based on composites of P3HT and TiO_2 nanoparticles. The transfer characteristic of each device exhibits a parallel shift to a positive gate voltage under light illumination. The device shows high photosensitivity, fast response, and stable performance under the illumination of both visible and UV light. Therefore, it is promising in the applications as low cost photosensors. Based on the same principle, OPTs based on the composites of various semiconducting polymers and semiconducting nanoparticles can be developed for sensing different wavelengths.

ACKNOWLEDGMENTS

The authors would like to acknowledge the help from Zhenghua Sun on the experiment. This work is financially supported by the Research Grants Council (RGC) of Hong Kong, China (Grant No. B-Q10T) and the Hong Kong Polytechnic University (Grant No. J-BB9S).

[1] H. Sirringhaus, Adv. Mater. **17**, 2411 (2005).
[2] B. Park, P. Paoprasert, I. In, J. Zwickey, P. E. Colavita, R. J. Hamers, P. Gopalan, and P. Evans, Adv. Mater. **19**, 4353 (2007).
[3] S. M. Mok, F. Yan, and H. L. W. Chan, Appl. Phys. Lett. **93**, 023310 (2008).
[4] T. Someya, T. Sekitani, S. Iba, Y. Kato, H. Kawaguchi, and T. Sakurai, Proc. Natl. Acad. Sci. U.S.A. **101**, 9966 (2004).
[5] H. Fukuda, Y. Yamagishi, M. Ise, and N. Takano, Sens. Actuators B **108**, 414 (2005).
[6] J. T. Mabeck and G. G. Malliaras, Anal. Bioanal. Chem. **384**, 343 (2006).
[7] F. Yan, P. Estrela, Y. Mo, P. Migliorato, H. Maeda, S. Inoue, and T. Shimoda, Appl. Phys. Lett. **86**, 053901 (2005).
[8] F. Yan, S. M. Mok, J. J. Yu, H. L. W. Chan, and M. Yang, Biosens. Bioelectron. **24**, 1241 (2009).
[9] P. Estrela, A. G. Stewart, F. Yan, and P. Migliorato, Electrochim. Acta **50**, 4995 (2005).
[10] S. M. Sze, *Physics of Semiconductor Devices*, 2nd ed. (Wiley, New York, 1981).
[11] H. Sirringhaus, T. Kawase, R. H. Friend, T. Shimoda, and M. Inbasekaran, Science **290**, 2123 (2000).
[12] M. A. Romero, M. A. G. Martinez, and P. R. Herczfeld, IEEE Trans. Microwave Theory Tech. **44**, 2279 (1996).
[13] M. Debucquoy, S. Verlaak, S. Steudel, K. Myny, J. Genoe, and P. Heremans, Appl. Phys. Lett. **91**, 103508 (2007).
[14] Y. T. Noh and D. Y. Kim, Solid-State Electron. **51**, 1052 (2007).
[15] B. Park, P. Paoprasert, I. In, J. Zwickey, P. E. Colavita, R. J. Hamers, P. Gopalan, and P. Evans, Adv. Mater. **19**, 43553 (2007).

[16]Y. Hu, G. Dong, C. Liu, L. Wang, and Y. Qiu, Appl. Phys. Lett. **89**, 072108 (2006).
[17]V. Podzorov and M. E. Gershenson, Phys. Rev. Lett. **95**, 016602 (2005).
[18]Y. Y. Noh, D. Y. Kim, Y. Yoshida, K. Yase, B. J. Jung, and E. Lim, Appl. Phys. Lett. **86**, 043501 (2005).
[19]T. P. I. Saragi, K. Onken, I. Suske, T. Fuhemann-Lieker, and J. Salbeck, Opt. Mater. (Amsterdam, Neth.) **29**, 1332 (2007).
[20]T. P. I. Saragi, R. Pudzich, T. Fuhrmann, and J. Salbeck, Appl. Phys. Lett. **84**, 2334 (2004).
[21]M. C. Hamilton, S. Martin, and J. Kanicki, IEEE Trans. Electron Devices **51**, 877 (2004).
[22]K. S. Narayan and N. Kumar, Appl. Phys. Lett. **79**, 1891 (2001).
[23]N. Marjanovic, T. B. Singh, G. Dennler, S. Gunes, H. Neugebauer, N. S. Sariciftci, R. Schwodiauer, and S. Bauer, Org. Electron. **7**, 188 (2006).
[24]J. Boucle, S. Chyla, M. S. P. Shaffer, J. R. Durrant, D. D. C. Bradley, and J. Nelson, Adv. Funct. Mater. **18**, 622 (2008).
[25]Y. Y. Lin, T. H. Chu, S. S. Li, C. H. Chuang, C. H. Chang, W. F. Su, C. P. Chang, M. W. Chu, and C. W. Chen, J. Am. Chem. Soc. **131**, 3644 (2009).
[26]F. Yan, P. Migliorato, and R. Ishihara, Appl. Phys. Lett. **88**, 153507 (2006).
[27]N. G. Park, J. Lagemaat, and A. J. Frank, J. Phys. Chem. B **104**, 8989 (2000).
[28]F. Yan, Y. Hong, and P. Migliorato, J. Appl. Phys. **101**, 064501 (2007).
[29]M. C. J. M. Vissenberg and M. Matters, Phys. Rev. B **57**, 12964 (1998).
[30]P. Peumans and S. R. Forrest, Chem. Phys. Lett. **398**, 27 (2004).